# Engineering polymer glue towards 90% zinc utilization for 1,000 hours to make high-performance Zn-ion batteries

*Yiding Jiao, Fangyan Li, Xin Jin, Qingsong Lei, Luhe Li, Lie Wang, Tingting Ye, Er He, Jiacheng Wang, Hao Chen, Jiang Lu, Rui Gao, Qianming Li, Chang Jiang, Jianwei Li, Guanjie He, Meng Liao, Huigang Zhang, Ivan P. Parkin, Huisheng Peng*, and Ye Zhang**

Y. Jiao, F. Li, X. Jin, Q. Lei, L. Li, Dr. L. Wang, T. Ye, E. He, J. Wang, H. Chen, J. Lu, R. Gao, Q. Li, C. Jiang, Prof. H. Zhang, Prof. Y. Zhang
College of Engineering and Applied Sciences, National Laboratory of Solid State Microstructures, Jiangsu Key Laboratory of Artificial Functional Materials, Chemistry and Biomedicine Innovation Center, Collaborative Innovation Center of Advanced Microstructures, Nanjing University
Nanjing 210023, China
E-mail: yezhang@nju.edu.cn

Y. Jiao, Dr. J. Li, Dr. G. He, Prof. I. P. Parkin
Christopher Ingold Laboratory, Department of Chemistry
University College London
London WC1H 0AJ, UK.

Dr. M. Liao, Prof. H. Peng
State Key Laboratory of Molecular Engineering of Polymers, Department of Macromolecular Science and Laboratory of Advanced Materials, Fudan University
Shanghai 200438, China
E-mail: penghs@fudan.edu.cn.

**Keywords:** polymer glue, zinc anodes, zinc utilization, zinc-ion batteries

**Abstract:** Zinc (Zn) metal is considered the promising anode for “post-lithium” energy storage due to its high volumetric capacity, low redox potential, abundant reserve, and low cost. However, extravagant Zn is required in present Zn batteries, featuring low Zn utilization rate and device-scale energy/power densities far below theoretical values. The limited reversibility of Zn metal was attributed to the spontaneous parasitic reactions of Zn with aqueous electrolytes, *i.e.*, corrosion with water, passive by-product formation and dendrite growth. Here, we design a new ion-selective polymer glue coated on Zn anode, isolating the Zn anode from the electrolyte by blocking water diffusion while allowing rapid $Zn^{2+}$ ion migration and facilitating uniform electrodeposition. Hence, a record-high Zn utilization of 90% was realized for 1,000 hours at high current densities, in sharp contrast to much poorer cyclability (usually < 200 hours) at lower Zn utilization (50–85%) reported to date. When matched with the vanadium-based cathode, the resulting Zn-ion battery exhibited an ultrahigh device-scale energy density of 228 $Wh \cdot kg^{-1}$, comparable to commercial lithium-ion batteries.

## 1. Introduction

The rapid development in portable electronics, electric vehicles and large-scale energy storage has witnessed the flourishing of lithium-ion batteries in the past decades.[1] However, defects in safety, high fabrication cost and raw material scarcity herald their pessimistic future.[2] Zn metal is endowed with intrinsic merits of high volumetric capacity (5,851 $mAh\cdot cm^{-3}$ *vs.* 2,046 $mAh\cdot cm^{-3}$ of Li), low redox potential (–0.76 V *vs.* standard hydrogen electrode), natural abundance (70 ppm *vs.* 20 ppm of Li in Earth's crust), safety and nontoxicity.[3] Therefore, Zn metal-based batteries, *e.g.,* Zn-ion batteries, are expected as the next-generation energy storage system.

However, an excessive amount of Zn is required for up-to-date Zn metal-based batteries, featuring insufficient Zn utilization (typically < 5%).[3a, 4] As a result, the full batteries suffer from device-scale energy and power densities far below theoretical values as well as poor cyclability. Recently, progress has been made in improving the Zn utilization by constructing Zn hosts with expanded surfaces,[5] designing functional surface coatings,[6] and modulating electrolytes with additives.[7] Nevertheless, at high Zn utilization of over 50%, the cycling stability was significantly impaired to less than 200 hours, impeding the desiring long-term application of Zn metal-based batteries.

The limited Zn reversibility and poor cycling stability were due to the spontaneous parasitic reactions of Zn with the aqueous electrolyte, including the corrosion with water, passive by-product formation and dendrite growth (**Figure 1a**).[8] The direct contact with aqueous electrolyte causes spontaneous hydrogen evolution, competes with Zn plating, and consumes Zn reserve. Parallelly, the resulting pH rise of the aqueous electrolyte leads to the formation of passive layers on the surface of Zn, diminishing the reactivity of the Zn anode. Moreover, induced rough surface with charge concentration contributes to eventual dendrite growth. The loose dendrites with more contact areas, in turn, intensify the corrosion behavior.[9]

Here, we design a new ion-selective polymer glue to enable an ultrahigh Zn utilization of 90% at a high current of 5 $mA\cdot cm^{-2}$ with superior cycling stability for 1,000 hours, far exceeding the performance of available Zn anode strategies, which can be ascribed to the simultaneous inhibition of corrosion, passivation, and dendrite growth (**Figure 1b**). The modified Zn anode was paired with $NH_4V_4O_{10}$ cathode to deliver a superior device-scale energy density of 228 $Wh\cdot kg^{-1}$ at 0.1 $A\cdot g^{-1}$ and power density of 2,533 $W\cdot kg^{-1}$ at 5.0 $A\cdot g^{-1}$ with outstanding rate performance and cyclability of 2,000 cycles with almost no decay.

## 2. Results and Discussion

### 2.1 Electrochemical Properties of Symmetric Batteries with Polymer Glue-Coated Zn Anodes

The polymer glue was prepared *via* co-dissolution of polyethylene oxide (PEO) and lithium bis(trifluoromethanesulfonyl)imide in a binary solvent consisting of acetone and dichloromethane, producing a viscous and glutinous texture (**Figure S1**).[10] The as-prepared polymer glue was then evenly coated on Zn foil by a simple doctor-blade method. The glutinous coating delivered a dense and compact surface with homogeneous elemental distribution, verified by both scanning electron microscopy and energy dispersive spectroscopy (**Figure S2**). The optimized thickness of the polymer glue on Zn anode was obtained from coulombic efficiency and electrochemical impedance, which was ~150 μm in this work (**Figure S3**).

The electrochemical performance of the polymer glue-modified Zn anode was evaluated by galvanostatic charge-discharge cycling in symmetric batteries. As shown in **Figure 2a**, the as-fabricated symmetric battery exhibited highly stable voltage profiles for 1,000 hours at high current of 5 $mA\cdot cm^{-2}$ with an ultrahigh Zn utilization. In comparison, the symmetric battery from bare Zn could only work for one cycle. It should be noted that the initial high voltage hysteresis originated from the $Zn^{2+}$ filling-up process in the polymer glue. In the subsequent cycles, the polymer glue was occupied with $Zn^{2+}$ ions. Thus, the electrodeposition could directly occur on the surface of Zn, leading to the lower voltage hysteresis. Cyclic voltammetry was conducted to investigate Zn stripping/plating reversibility, which confirmed increased peak current and reduced polarization for polymer glue-coated Zn foil (**Figure S4**). Moreover, the strategy of polymer glue was also effective in other electrolyte systems, such as 3 M $Zn(OTf)_2$ electrolyte (**Figure S5**).

Excellent rate performance was also observed for the polymer glue-coated Zn anode. At increasing current densities from 2 to 10 $mA\cdot cm^{-2}$, stable voltage-time curves were obtained with a minor increase in overpotential (**Figure 2b**). The capability of cycling at high current benefits the application requiring high power output. Furthermore, to systematically investigate the electrochemical performance of polymer glue-coated Zn anode at different utilization rates, the symmetric batteries were further tested at increasing Zn utilization rates from 10% to 80%, and steady voltage profile and gradually reducing overpotentials were perceived (**Figure S6**). To the best of our knowledge, the polymer glue here offers the Zn anode with the highest Zn utilization rate at a remarkably high current to date. Besides, the cycling time was significantly prolonged while the voltage hysteresis was adequately controlled, demonstrating its effectivity as a high-performance Zn anode for Zn-ion batteries (**Figure 2c** and **Table S1**).[5a-d, 6-7]

### 2.2 Suppression of Corrosion by Polymer Glue

The underlying mechanism behind the excellent performance was systematically explored. The excellent rate performance of the symmetric batteries could be ascribed to the fast $Zn^{2+}$ ion migration capability provided by the polymer glue. The ionic conductivity of polymer glue reached 6.18 $mS{\cdot}cm^{-1}$, which was a 1,400-fold increase compared to PEO (**Figure S7**). The cation transference number was measured to identify the contribution of $Zn^{2+}$ ions in the total electric current for the polymer glue and pristine PEO. The transference number for the polymer glue was calculated as 0.98, which far exceeded that of pristine PEO (**Figure S8** and **S9**). The enhanced ionic conductivity and transference number jointly proved fast Zn stripping/plating kinetics and favored the use of Zn anode at high current densities. The enhanced $Zn^{2+}$ conductivity was presumably due to the decreased crystallinity from PEO and lithium bis(trifluoromethanesulfonyl)imide (**Figure S10**), anion-fixing effect and $Zn^{2+}$ percolation.[11] The typical broad amorphous scattering peak observed for the polymer glue corresponded to the broad distribution of interchain distances (*i.e.*, the radical distribution function), resulted from the interaction of $Li^+$ ions and PEO chains.[10] $Zn^{2+}$ ions were liable to migrate *via* oxygen atoms in ether groups and enable high ionic conductivity,[12] verified by the varying chemical environment of such oxygen atoms (**Figure S11**). Characteristic peaks at 840 $cm^{-1}$ and 860 $cm^{-1}$ related to C-O stretch and $CH_2$ rock modes in PEO disappeared. In contrast, the peak at 863 $cm^{-1}$ to coordinate solvated cations and polymer ether oxygens was strengthened.[13] The diffusion coefficient of $Zn^{2+}$ was simulated from molecular dynamics, which was as high as $1.00 \times 10^{-5}$ $cm^2{\cdot}s^{-1}$, corresponding to the experimental evidence (**Figure 3a** and **S12**).

Despite the enabled fast $Zn^{2+}$ migration, $H_2O$ penetration was significantly impeded. Similarly, the diffusion coefficient of water into polymer glue was simulated from molecular dynamics, which was calculated to be $1.01 \times 10^{-7}$ $cm^2{\cdot}s^{-1}$ and 1/100 lower than that of the polymer glue (**Figure 3b** and **S13**). The underlying mechanism for the prevention of water penetration was verified by detecting the O composition at increasing depths of the soaked polymer glue-coated Zn foil from X-ray photoelectron spectroscopy. The characteristic peak at ~530 eV corresponding to lithium hydroxide gradually disappeared with increasing etching depths to 240 nm. This demonstrated the formation of PEO-$Li^+$-$H_2O$ complex, which confined the absorbed $H_2O$ molecules along the PEO chain and hampered their free movements (**Figure S14**).[14]

The strong adherence between the polymer glue and Zn anode was the other guarantee for the constant protection from the electrolyte, confirmed by standard peeling tests. The adhesion strength reached a high value of 83 $N{\cdot}m^{-1}$, corresponding with the sticky interface depicted in the inset photograph (**Figure 3c**). The strong adhesion was further verified by testing the shear stress between the polymer glue and Zn foil, which reached 37 kPa at a constant tensile rate of 50 mm·min$^{-1}$ (**Figure S15**). The adhesiveness originated presumably from the inter-molecular force within PEO and between PEO and Zn foil.

Corrosion and passivation were thereby constantly and significantly inhibited with the suppressed $H_2O$ penetration as well as the adherent and compact interface. As shown in **Figure 3d**, linear polarization tests were used to measure the corrosion rate. Compared with the bare Zn, the corrosion current density with the use of polymer glue was 5.25 times lower, indicating suppressed corrosion behavior (**Figure S16**). The anti-corrosion performance of polymer glue was evaluated by soaking both glue-coated and bare Zn anodes in mild acid $ZnSO_4$ electrolyte. Optical microscopy was used to monitor the $H_2$ evolution on Zn in 30 minutes. No $H_2$ bubbles were observed from the glue-coated Zn anode (**Figure 3e**) due to the adequate protection of the polymer glue, while many $H_2$ bubbles were spotted on the bare Zn (**Figure 3f**). During the corrosion, protons in the electrolyte were consumed, leading to increased pH values during cycling. Therefore, the corrosion rate can be monitored by measuring the pH of the electrolyte of symmetric batteries to compare the polymer glue-coated and bare Zn foils (5 mA·cm$^{-2}$). In 10 cycles, the pH remained almost unchanged for the polymer glue-coated Zn whereas the pH was increased by 0.5 for the bare Zn owing to intense corrosion (**Figure 3g** and **3h**). The deposited Zn was sandwiched between the polymer glue and Zn substrate, referring to the Zn substrate coated directly with polymer glue (**Figure S17**). The constant isolation of Zn anode from the aqueous electrolyte during cycling was thus achieved.

### 2.3 Suppression of Passive Layer Formation and Dendrite Growth by Polymer Glue

The passivation-inhibition property was further investigated by surface analysis. The metallic luster of Zn protected by polymer glue was well maintained after being immersed in $ZnSO_4$ electrolyte for 15 days, while a rusty passive layer was gradually formed on the bare Zn foil (**Figure S18**). X-ray diffraction was further used to probe the crystallography of the passivation product as $Zn_4SO_4(OH)_6{\cdot}5H_2O$ (PDF#00-039-0688) (**Figure 4a**). The anti-passivation behavior was also observed in symmetric batteries. The composition remained unaltered for the Zn anode with the polymer glue after soaking in an aqueous electrolyte for 7 days. For the polymer glue-protected Zn anode, the Zn composition remained as $Zn^0$ after deep cycling 6 times, and it was the same for O and S composition. By contrast, for cycled bare Zn anode, $Zn^{II}$ peak, O species corresponding to $SO_4^{2-}$ and complex S species were observed, demonstrating the passivized anodic surface for unprotected Zn anode (**Figure 4b-d**).

The surface morphology of the Zn anode after cycling was investigated by scanning electron microscopy. A uniform dendrite-free surface was detected for the polymer-glue-coated Zn, which effectively eliminated the short circuit induced by dendrite growth (**Figure 4e**). On the contrary, a dendritic surface was noted for cycled bare Zn anodes (**Figure 4f**), in sharp contrast with the pristine Zn foil (**Figure S19**). The ever-growing dendrites were responsible for separator penetration and consequent short circuit. Meanwhile, the enlarged surface area intensified corrosion and passivation, leading to an overall low Zn utilization rate. The difference in crystallographic orientation was validated with X-ray diffraction (**Figure S20**). The surface-preferred dendrite-free (002) crystal plane was well maintained for Zn foils protected with the polymer glue. At the same time, more (100) orientation was exposed for bare Zn, corresponding to extravagant dendrites observed.[15]

The possible explanation for the unique Zn deposition behavior was explored with chronoamperometry tests in symmetric batteries (**Figure S21**). The varied current densities at a constant overpotential depicted the electrodeposition process.[16] The current density observed from polymer glue-coated Zn anode was well maintained at $-4.25\ \mathrm{mA\cdot cm^{-2}}$, indicating the local reduction of $Zn^{2+}$ ions with constrained lateral diffusion. The constrained lateral diffusion was anticipated because the firmly adhered polymer glue provided excessive energy barriers for lateral movement of the absorbed $Zn^{2+}$, which was demonstrated with the reduced ionic conductivity. Therefore, these $Zn^{2+}$ ions were kinetically favorable to be reduced and deposited proximately, producing many nucleation sites, and growing into uniform and dendrite-free anodic surface.[6b] By contrast, at a constant overpotential of $-150$ mV, the current densities gradually increased from $-4.2$ to $-5.5\ \mathrm{mA\cdot cm^{-2}}$ in 60 seconds for bare Zn anodes. The escalating current density represented the reduced nucleation difficulty. A probable cause was that due to the “tip effect”, $Zn^{2+}$ ions were liable to migrate laterally along the surface of Zn anodes and accumulate on the protruding active sites, which in turn exaggerated the unevenness of the electric field and lowered the energy barrier of further Zn deposition (**Figure 4g**).[17]

### 2.4 Electrochemical Properties of Full Batteries with $NH_4V_4O_{10}$ and Polymer Glue-Coated Zn

Vanadium-based cathode materials have attracted increasing interest due to their ultrahigh specific capacity and cycling stability.[3b, 3c] Despite their comparatively lower discharge potential, the specific capacity of vanadium-based materials is much higher than manganese-based materials, which are ideal for exploring the performance of polymer glue-assisted Zn anodes.[18] Therefore, here, $NH_4V_4O_{10}$ cathode was paired with the polymer glue-coated Zn anode to fabricate full Zn-ion batteries (**Figure S22**). Cyclic voltammetry was conducted to examine the energy storage kinetics after introducing the polymer glue on the Zn anode. The reversible reaction was well restored with almost no polarization. Moreover, the integral area of the cyclic voltammograms increased gradually during cycling at a scan rate of 0.2 mV·s$^{-1}$, indicating that $NH_4V_4O_{10}$ cathode experienced an electrochemical activation process when pairing with polymer glue-coated Zn anode, ensuring its high-capacity output (**Figure S23**).

The full Zn-ion battery exhibited an ultrahigh specific capacity of 410 mAh·g$^{-1}$ based on the active mass of the cathode even at an ultrahigh Zn utilization rate of 50%. In contrast, the capacity faded dramatically in the first few cycles for bare Zn anodes (**Figure 5a**). To be noted, the initial capacity growing was attributed to the activation of cathode, presumably due to crystallinity and morphology optimization.[19] The voltage-capacity curves of the 1st and 10th cycles were selected to analyze the mechanism of battery failure. The voltage profile was well restored after 10 working cycles with ~33% capacity improvement for the full Zn-ion battery with polymer glue-protected Zn anode. While for full Zn-ion battery with bare Zn anode, voltage fluctuation during discharging (Zn stripping from anode) at the 10th cycle was spotted, implying that the shortage of Zn led to the eventual battery malfunction (**Figure 5b**). To study the cycling capability, the full battery from $NH_4V_4O_{10}$ and polymer glue-coated Zn was cycled at a high rate of 5.0 A·g$^{-1}$. As shown in **Figure 5c**, the use of polymer glue-coated Zn afforded a significantly enhanced cycling stability over 2,000 cycles. Contrastingly, the full battery capacity with bare Zn anode faded rapidly to ~20% in the first 500 cycles.

To evaluate the rate performance, the full batteries from $NH_4V_4O_{10}$ and the polymer glue-coated Zn were cycled stepwise at increasing current densities of 0.1 to 5.0 A·g$^{-1}$ (based on the active mass of cathode). The capacity retention was measured to be 30% at 5.0 A·g$^{-1}$, delivering a superior rate capability (**Figure 5d**). The energy density was calculated as 228 Wh·kg$^{-1}$ at 0.1 A·g$^{-1}$ and power density was 2,533 W·kg$^{-1}$ at 5.0 A·g$^{-1}$ based on the total mass of cathode and anode from **Figure 5d** and compared at **Table S2** and in **Figure 5e**. Our Zn-ion batteries much exceed the reported aqueous counterpart.[5b, 5c, 20] Besides, our Zn-ion batteries further show both high energy and power densities than commercialized energy storage systems (**Figure S24**).

An outlook for the practical application of the polymer glue-based Zn-ion batteries was further provided. The preparation process of the polymer glue and modified Zn anode was based on co-dissolution of raw materials and blade coating process, which are very simple and compatible with the equipment currently available in the industry. By simply multiplying the amount of polymer glue and Zn foil, we had produced a massive polymer glue-coated Zn foil (**Figure 6a**). A pouch cell was designed by sandwiching a polymer glue-coated Zn foil in a “U”-shaped cathode made by coating $NH_4V_4O_{10}$ on 316 stainless steel mesh (**Figure 6b**). The as-fabricated pouch cell could effectively power a smartphone (**Figure 6c**).

In contrast with other rigid protections, the polymer glue was intrinsically flexible, providing constant protection for the Zn anode at the bending state. Therefore, a pouch cell from polymer glue-coated Zn anode could bear bending at 90° for 1,000 cycles, with capacity retention up to 95% (**Figure 6d**). Safety issue such as combustion and explosion of non-aqueous batteries have restrained their application scenarios. In contrast, the as-prepared pouch cell from polymer-glue coated Zn foil could work continuously and power a liquid-crystal display after being cut (**Figure 6e**). Thermal imaging illuminated that the temperature remained unaltered in the process of cutting (**Figure 6f**).

## 3. Conclusion

In summary, we have designed a new polymer glue on Zn anode, enabling 90% Zn utilization at an elevated current density of 5 $mA\cdot cm^{-2}$ for an ultralong time of 1,000 hours. The working mechanism of the polymer glue was systematically explored, demonstrating the effective inhibition of corrosion and passivation of Zn anode by simultaneously blocking $H_2O$ penetration while facilitating fast $Zn^{2+}$ ion migration. Moreover, the polymer glue constrains the lateral accumulation of $Zn^{2+}$ ions and facilitates uniform and dendrite-free Zn deposition. Therefore, the resulting full battery exhibited ultrahigh energy and power densities with a long lifespan. This work represents a general and efficient strategy in developing the next-generation aqueous batteries aiming at high electrochemical properties.

## 4. Experimental Section

*Preparation of Polymer Glue-Coated Zn Electrodes*: All chemicals, including polyethylene oxide (PEO, Mw of 600,000, Aladdin), lithium bis(trifluoromethanesulfonyl)imide (LiTFSI, Aladdin), dichloromethane ($CH_2Cl_2$, Aladdin) and acetone (Sinopharm), were commercially available and used as received. The polymer glue was prepared by dissolving 1.4 g PEO and 1.2 g LiTFSI in 10 mL acetone/$CH_2Cl_2$ binary solvent with a mass ratio of 1:40 and stirring vigorously overnight at 40 °C. The PEO film as the control group was prepared by dissolving 1.4 g PEO into 10 mL acetone/$CH_2Cl_2$ binary solvent with a mass ratio of 1:40 and subsequently evaporating the solvent in ambient air. The polymer glue-coated Zn electrodes were prepared by the doctor-blade method. Specifically, the Zn anode was firstly cut from Zn foils with a diameter of 16 mm, followed by scraping a thin layer of polymer glue with controlled thickness. The polymer-glue coated Zn anode was allowed to stand for 30 minutes to evaporate the excess solvent.

*Synthesis of $NH_4V_4O_{10}$*: $NH_4V_4O_{10}$ was synthesized by a single-step hydrothermal reaction. In a typical process, 5 mmol of ammonium metavanadate ($NH_4VO_3$, Macklin) was dissolved into 30 mL of deionized water and stirred for 15 minutes under an ambient environment. 2 mmol of oxalic acid (Macklin) was added to the above solution with additional violent stirring for 40 minutes. The as-prepared solution was then transferred into a Teflon-lined autoclave (50 mL) and heated at 180 °C for 6 hours. The obtained precipitate was washed with deionized water at least three times and collected with a centrifuge and vacuum dried at 60 °C overnight.

*Assembly of Symmetric Batteries*: The symmetric battery was fabricated by pairing two polymer glue-coated Zn electrodes (diameter of 16 mm) in CR2032 coin cells. The thicknesses of the used Zn foil were 10 and 20 μm at 80% and 90% Zn utilization rate, respectively. Two layers of glass fiber filters (GF/A, Whatman) were used as the separator. The electrolytes were prepared by dissolving Zn sulfate heptahydrate ($ZnSO_4\cdot7H_2O$, Sinopharm) or Zn trifluoromethanesulfonate ($Zn(OTf)_2$, Macklin) into deionized water to form 2 M $ZnSO_4$ or 3 M $Zn(OTf)_2$ electrolytes. The volume of the electrolyte was fixed to 300 μL.

*Assembly of Zn-$NH_4V_4O_{10}$ Coin Cells*: $NH_4V_4O_{10}$, Super P conductive agent (Imerys, Super P Li) and poly(vinylidene fluoride) (PVDF, Macklin) were mixed and ground in a mortar with mass ratios of 7:2:1. The cathode slurry was prepared by adding the proper amount of N-methyl-pyrrolidone (NMP, Macklin). The as-prepared slurry was evenly coated on hydrophilic carbon fiber paper (diameter of 14 mm, Toray) and vacuum dried at 60 °C overnight. The mass loadings were measured to be 2–3 $mg\cdot cm^{-2}$. The cathode was assembled in a CR2032 coin cell with bare or polymer glue-coated Zn foils (1/4 of a circle with a diameter of 16 mm, the thickness of 10 μm, and average Zn mass of 3.75 mg) as the anode. Two layers of glass fiber filters (GF/A, Whatman Ltd.) were used as the separator. The electrolytes were prepared by dissolving $Zn(OTf)_2$ into deionized water to form 3 M $Zn(OTf)_2$ electrolytes. The volume of the electrolyte was fixed to 300 μL.

*Assembly of Zn-$NH_4V_4O_{10}$ Pouch Cells*: The cathode slurry was prepared by the same procedure above. The as-prepared slurry was evenly coated on 316 stainless steel mesh (6 cm × 8 cm) and dried in a vacuum oven at 60 °C overnight. The mass loadings were measured to be 2–3 $mg\cdot cm^{-2}$. The cathode was assembled with the polymer glue-coated Zn foil (4 cm × 6 cm, the thickness of 40 μm, and average Zn mass of 800 mg) and 3 M $Zn(OTf)_2$

aqueous electrolyte in ambient air. Two layers of glass fiber filters (GF/A, Whatman Ltd.) were used as the separator. The as-prepared pouch cell was sealed with aluminum-plastic film.

*Characterizations*: The optical microscopy image was obtained using an inverted microscope Axio Vert.A1 FL-LED (Zeiss). Raman spectra were characterized with LabRAM HR evolution confocal Raman microscope (HORIBA) at 532 nm and 100% intensity. The X-ray diffraction pattern was obtained with LabX XRD-6100 X-ray Diffractometer (Shimadzu). The morphologies were analyzed by S-4800 (Hitachi) and Sigma 500 (Zeiss) field emission scanning electron microscope. X-ray photoelectron spectroscopy study was made at VersaProbe III Scanning XPS Microprobe (Physical Electronics). All the samples were recovered for X-ray diffraction, Scanning Electron Microscopy and X-ray photoelectron spectroscopy were recovered from a full aqueous battery in a CR2032 coin-cell configuration after electrochemical cycling. To measure the adhesion between the polymer glue and Zn, the polymer glue was first coated onto a flexible polyethylene terephthalate (PET) substrate with an adhesion area of 1 cm × 4 cm. The polymer glue-coated PET was then attached face-to-face with the Zn foil and tested with a mechanical testing instrument (50N load-cell, HY-0580). The peel-off and shear modes were used to measure the adhesion. For peel-off mode, the above film was peeled off from the Zn foil from the same side, and the adhesion was calculated by dividing the average force at constant state by the width of the adhesion area. For shear mode, the above film and the Zn foil were sheared at 180°, and the adhesion was calculated by dividing the maximal force by the adhesion area. All tests were conducted with a constant tensile speed of 50 $mm \cdot min^{-1}$.

*Electrochemical Measurements*: To measure the corrosion rate in 2 M $ZnSO_4$ electrolyte, a three-electrode configuration was utilized with bare or polymer glue-coated Zn as working electrode, Pt foil as counter electrode and saturated calomel electrode as reference electrode. A linear polarization test was carried out at a scan rate of 5 $mV \cdot s^{-1}$ from −0.6 to −2.0 V *vs.* saturated calomel electrode with CS350 Potentiostats (CorrTest). The current density was obtained by dividing the measured current by active surface area of bare or polymer glue-coated Zn. To determine the ionic conductivity, PEO film or polymer glue layer was sandwiched by two stainless steel foil (each with the thickness of 100 μm). Electrochemical impedance spectroscopy was performed with CS350 Potentiostats (CorrTest). The frequency range was from 50,000 to 0.01 with an amplitude of 10 mV. The open-circuit potential was set as the initial voltage. The ionic transference number was determined by following the classic electrochemical measurement. Firstly, a three-electrode system was established with polymer glue/PEO-coated or bare Zn foils as working and counter electrodes and saturated calomel electrode as reference electrode. Secondly, electrochemical impedance spectroscopy was conducted to measure the initial resistance ($R_0$) with a frequency range from 50,000 to 0.01 with an amplitude of 10 mV. The open-circuit potential was set as the initial voltage. Then, chronoamperometry was carried out with an overpotential ($\Delta V$) of 10 mV for 6000 seconds. The initial current ($I_0$) and steady-state current ($I_s$) were recorded. Lastly, electrochemical impedance spectroscopy was conducted again to obtain the steady-state resistance ($R_s$) under the same conditions. The reversibility of Zn stripping/plating was detected by establishing a three-electrode system with bare stainless-steel foil (thickness of 100 μm and area of 2 $cm^2$) or stainless-steel foil protected with polymer glue as working electrode, Zn foil (thickness of 100 μm and area of 2 $cm^2$) as counter electrode and saturated calomel electrode as reference electrode. Cyclic voltammetry was conducted in 2 M $ZnSO_4$ electrolyte at a scan rate of 5 $mV\cdot s^{-1}$ from −0.6 to −1.2 V with CS350 Potentiostats (CorrTest). Galvanostatic cycling tests were carried out with a LANHE CT2001 (LAND Electronic Co. Ltd.) battery testing system. Galvanostatic cycling of symmetric batteries was carried out with a LANHE CT2001 battery testing system (LAND Electronics). The control parameter for each cycle was set according to the intended capacity at a specific Zn utilization rate. The symmetric batteries were initially charged. For pH monitoring, a two-electrode configuration was established in a 50 mL cell with one Zn foil (thickness of 100 μm) as working electrode and another Zn foil (thickness of 100 μm) as counter and reference electrodes. The tests were carried out with CS350 Potentiostats (CorrTest). The current density for galvanostatic cycling was 5 $mA\cdot cm^{-2}$. After each cycle, the electrolyte was stirred vigorously, after which a pH probe was used to detect the pH of the electrolyte. To analyze the possible cause for the unique Zn deposition morphology, a three-electrode configuration was established in a 50 mL cell with either bare or polymer glue-coated Zn foil (thickness of 100 μm) as both working and counter electrodes and saturated calomel electrode as reference electrode. The chronoamperometry tests were conducted with CS350 Potentiostats (CorrTest) with an overpotential of −150 mV. The cyclic voltammetry for Zn-$NH_4V_4O_{10}$ full batteries was conducted in CR2032 coin cells from 0.3 to 1.7 V at 0.2 $mV\cdot s^{-1}$ with CS350 Potentiostats (CorrTest). Galvanostatic cycling of Zn-$NH_4V_4O_{10}$ full batteries was carried out with a LANHE CT2001 battery testing system (LAND Electronics). The batteries were initially discharged to 0.3 V and then charged back to 1.7 V at specific current densities.

*Simulation*: The model of 30 PEO polymer chains with 30 repeated units and 60 $Zn(TFSI)_2$ was built by Packmol[21] to represent the polymer glue. In addition, 20 water molecules were inserted into the polymer glue. The model was annealed from 700 K to 298 K at 1 atms to stretch the PEO segments fully. A further 500 ps molecular dynamics simulation was conducted at 298.15 K and 1 atms to track changes in each system. After the density of all systems was remained stable, a sample of 300 ps was taken to calculate the mean square displacement (MSD). COMPASS force fields were used to perform the molecular simulations. The time step was fixed at 1.0 fs, and the temperature and pressure were controlled by Nosé-Hoover-Langevin. A van der Waals interaction cutoff of 1.5 nm was employed, and the Ewald method was used to account for the long-range electrostatic interactions.

*Calculation*: The ionic conductivity was calculated by the following equation,

$$\sigma = \frac{l}{R_{\Omega} \times S}$$

where $l$ is the measured thickness, $S$ is the facing area of the two stainless steel foil, and $R_{\Omega}$ is the horizontal intercept obtained from electrochemical impedance spectroscopy.

The ionic transference number was calculated by the following equation,

$$T = \frac{I_s \times (\Delta V - I_0 \times R_0)}{I_0 \times (\Delta V - I_s \times R_s)}$$

where $\Delta V$ is the polarization voltage; $I_0$ and $R_0$ are the initial current and resistance, respectively; $I_s$ and $R_s$ are the steady-state current and resistance.

Zn utilization rate was calculated by the following equation,

$$ZUR = \frac{C_{cycle}/C_{theoretica}}{m_{WE}} \times 100\%$$

where $C_{cycled}$ is the capacity set for galvanostatic cycling (in mAh), $C_{theoretical}$ is the theoretical gravimetric specific capacity of Zn (820 mAh·g$^{-1}$), and $m_{WE}$ is the mass of the Zn or polymer glue-coated Zn working electrode (unit of g).

The specific capacity of the Zn-$NH_4V_4O_{10}$ full battery was calculated based on the following equation,

$$C = \frac{\int i d\,t}{m_{NH_4V_4O_{10}}}$$

where $i$ is discharge current, $t$ is the discharge time, and $m_{NH4V4O10}$ is the mass of the active material on the $NH_4V_4O_{10}$ cathode.

The energy density of the Zn-$NH_4V_4O_{10}$ full battery was calculated based on the following equation,

$$E = \frac{C \times m_{NH_4V_4O_{10}} \times V}{m_{NH_4V_4O_{10}} + m_{Zn}}$$

where $C$ is the calculated specific capacity, $V$ is the operating voltage, $m_{NH4V4O10}$ is the mass of the active material on $NH_4V_4O_{10}$ cathode, and $m_{zn}$ is the mass of Zn anode.

Taking the mass of electrolyte and polymer glue into calculation,

$$E = \frac{C \times m_{NH_4V_4O_{10}} \times V}{m_{NH_4V_4O_{10}} + m_{Zn} + m_{electrolyte} + m_{PG}}$$

where $m_{electrolyte}$ is the mass of the electrolyte and $m_{PG}$ is the mass of polymer glue. The overall energy density and power density were calculated as 8.8 Wh·kg$^{-1}$ at 0.1 A·g$^{-1}$ and 98.4 W·kg$^{-1}$ at 5.0 A·g$^{-1}$,respectively.

The power density of the Zn-$NH_4V_4O_{10}$ full battery was calculated by the following equation,

$$P = \frac{E}{t}$$

where $E$ is the calculated energy density, and $t$ is the discharge time.

The mean square displacement (MSD) was calculated by the following equation,

$$MSD = \sum_{i}^{N} < |r_i(t) - r_i(0)|^2 >$$

where r is the position vector of particles, and $t$ is the simulation time.

The diffusion coefficient (D) was calculated by the following equation,

$$D = \frac{1}{6} \lim_{t\to\infty} \frac{d}{dt}(MSD)$$

*Application display*: To charge a smartphone, three as-prepared pouch cells were connected in series and linked to a TPS61088 boost converter (Shaibang Ltd.) and charged Huawei Nova 6. The flexibility of the as-prepared pouch cells was characterized by testing their specific capacities after 0, 200, 400, 600, 800 and 1000 bending cycles. The bending angle was controlled to 90°. The safety characterization was conducted by cutting an as-prepared pouch cell while connecting with an LED thermometer. The temperature of the battery during cutting is measured with an infrared camera (FORTRIC 225-1).

## Supporting Information

Supporting Information is available from the Wiley Online Library or from the author.

## Acknowledgements

This work was supported by the MOST (2016YFA0203302), National Natural Science Foundation of China (22005137), Natural Science Foundation of Jiangsu Province (BK20200321), Fundamental Research Funds for the Central Universities (14380187), National Postdoctoral Program for Innovative Talent (BX20200161) and Start-up Fund at Nanjing University (14912221). The authors acknowledge High Performance Computing Center, Nanjing University, for applying the FORCITE module in Material Studio. Y. Jiao thanks the funding support from China Scholarship Council/University College London for the joint PhD scholarship.

## Conflict of Interest

The authors declare no conflict of interest.

## References

[1] J. -M. Tarascon, M. Armand, *Nature* **2001**, *414*, 359.

[2] a) J. W. Choi, D. Aurbach, *Nat. Rev. Mater.* **2016**, *1*, 16013; b) J. Liu, Z. Bao, Y. Cui, E. J. Dufek, J. B. Goodenough, P. Khalifah, Q. Li, B. Y. Liaw, P. Liu, A. Manthiram, Y. S. Meng, V. R. Subramanian, M. F. Toney, V. V. Viswanathan, M. S. Whittingham, J. Xiao, W. Xu, J. Yang, X.-Q. Yang, J.-G. Zhang, *Nat. Energy* **2019**, *4*, 180.

[3] a) H. Dong, J. Li, J. Guo, F. Lai, F. Zhao, Y. Jiao, D. J. L. Brett, T. Liu, G. He, I. P. Parkin, *Adv. Mater.* **2021**, *33*, 2007548; b) X. Jia, C. Liu, Z. G. Neale, J. Yang, G. Cao, *Chem. Rev.* **2020**, *120*, 7795; c) L. E. Blanc, D. Kundu, L. F. Nazar, *Joule* **2020**, *4*, 771; d) Y. Gao, Z. Yan, J. L. Gray, X. He, D. Wang, T. Chen, Q. Huang, Y. C. Li, H. Wang, S. H. Kim, T. E. Mallouk, D. Wang, *Nat. Mater.* **2019**, *18*, 384; e) Q. Gui, Y. Feng, B. Chen, F. Gu, L. Chen, S. Meng, M. Xu, M. Xia, C. Zhang, J. Yang, *Adv. Energy Mater.* **2021**, *11*, 2003553; f) R. Lu, B. Zhang, Y. Cheng, K. Amin, C. Yang, Q. Zhou, L. Mao, Z. Wei, *J. Mater. Chem. A* **2021**, *9*, 10393.

[4] Z. Cao, P. Zhuang, X. Zhang, M. Ye, J. Shen, P. M. Ajayan, *Adv. Energy Mater.* **2020**, *10*, 2001599.

[5] a) W. Guo, Z. Cong, Z. Guo, C. Chang, X. Liang, Y. Liu, W. Hu, X. Pu, *Energy Stor. Mater.* **2020**, *30*, 104; b) Y. Zeng, X. Zhang, R. Qin, X. Liu, P. Fang, D. Zheng, Y. Tong, X. Lu, *Adv. Mater.* **2019**, *31*, 1903675; c) Y. Zhou, X. Wang, X. Shen, Y. Shi, C. Zhu, S. Zeng, H. Xu, P. Cao, Y. Wang, J. Di, Q. Li, *J. Mater. Chem. A* **2020**, *8*, 11719; d) Y. Zhou, X. Wang, X. Shen, Y. Shi, C. Zhu, S. Zeng, H. Xu, P. Cao, Y. Wang, J. Di, Q. Li, *J. Mater. Chem. A* **2020**, *8*, 11719; e) L. Kang, M. Cui, F. Jiang, Y. Gao, H. Luo, J. Liu, W. Liang, C. Zhi, *Adv. Energy Mater.* **2018**, 8, 1801090.

[6] a) M. Zhu, J. Hu, Q. Lu, H. Dong, D. D. Karnaushenko, C. Becker, D. Karnaushenko, Y. Li, H. Tang, Z. Qu, J. Ge, O. G. Schmidt, *Adv. Mater.* **2021**, *33*, 2007497; b) Z. Zhao, J. Zhao, Z. Hu, J. Li, J. Li, Y. Zhang, C. Wang, G. Cui, *Energy Environ. Sci.* **2019**, *12*, 1938; c) J. Hao, X. Li, S. Zhang, F. Yang, X. Zeng, S. Zhang, G. Bo, C. Wang, Z. Guo, *Adv. Funct. Mater.* **2020**, *30*, 2001263; d) Z. Cao, X. Zhu, D. Xu, P. Dong, M. O. L. Chee, X. Li, K. Zhu, M. Ye, J. Shen, *Energy Stor. Mater.* **2021**, *36*, 132; e) P. Cao, X. Zhou, A. Wei, Q. Meng, H. Ye, W. Liu, J. Tang, J. Yang, *Adv. Funct. Mater.* **2021**, *31*, 2100398; f) L. Ma, Q. Li, Y. Ying, F. Ma, S. Chen, Y. Li, H. Huang, C. Zhi, *Adv. Mater.* **2021**, *33*, 2007406; g) X. Xie, S. Liang, J. Gao, S. Guo, J. Guo, C. Wang, G. Xu, X. Wu, G. Chen, J. Zhou, *Energy Environ. Sci.* **2020**, *13*, 503; h) J. Y. Kim, G. Liu, G. Y. Shim, H. Kim, J. K. Lee, *Adv. Funct. Mater.* **2020**, *30*, 2004210; i) D. Lee, H.-I. Kim, W.-Y. Kim, S.-K. Cho, K. Baek, K. Jeong, D. B. Ahn, S. Park, S. J. Kang, S.-Y. Lee, *Adv. Funct. Mater.* **2021**, 2103850.

[7] a) Z. Hou, H. Tan, Y. Gao, M. Li, Z. Lu, B. Zhang, *J. Mater. Chem. A* **2020**, *8*, 19367; b) L. Ma, T. P. Pollard, Y. Zhang, M. A. Schroeder, M. S. Ding, A. V. Cresce, R. Sun, D. R. Baker, B. A. Helms, E. J. Maginn, C. Wang, O. Borodin, K. Xu, *Angew. Chem. Int. Ed.* **2021**, *60*, 12438; c) L. Cao, D. Li, T. Pollard, T. Deng, B. Zhang, C. Yang, L. Chen, J. Vatamanu, E. Hu, M. J. Hourwitz, L. Ma, M. Ding, Q. Li, S. Hou, K. Gaskell, J. T. Fourkas, X.-Q. Yang, K. Xu, O. Borodin, C. Wang, *Nat. Nanotechnol.* **2021**, DOI: 10.1038/s41565-021-00905-4.

[8] a) J. Hao, X. Li, X. Zeng, D. Li, J. Mao, Z. Guo, *Energy Environ. Sci.* **2020**, *13*, 3917. b) Q. Yang, Q. Li, Z. Liu, D. Wang, Y. Guo, X. Li, Y. Tang, H. Li, B. Dong, C. Zhi, *Adv. Mater.* **2020**, 32, 2001854.

[9] C. Li, X. Xie, S. Liang, J. Zhou, *Energy Environ. Sci.* **2020**, *3*, 146.

[10] M. Echeverri, N. Kim, T. Kyu, *Macromolecules* **2012**, *45*, 6068.

[11] Z. Li, H.-M. Huang, J.-K. Zhu, J.-F. Wu, H. Yang, L. Wei, X. Guo, *ACS Appl. Mater. Interfaces* **2019**, *11*, 784.

[12] a) D. J. Brooks, B. V. Merinov, W. A. Goddard, B. Kozinsky, J. Mailoa, *Macromolecules* **2018**, *51*, 8987; b) J. E. Bostwick, C. J. Zanelotti, C. Iacob, A. G. Korovich, L. A. Madsen, R. H. Colby, *Macromolecules* **2020**, *53*, 1405.

[13] L. Edman, *J. Phys. Chem. B* **2000**, *104*, 7254.

[14] X. Zhang, L. Zhou, Y. Wang, Q. Zhou, *Polym. Sci. Ser. A* **2018**, *60*, 50.

[15] M. Zhou, S. Guo, J. Li, X. Luo, Z. Liu, T. Zhang, X. Cao, M. Long, B. Lu, A. Pan, G. Fang, J. Zhou, S. Liang, *Adv. Mater.* **2021**, *33*, 2100187.

[16] C. J. Lan, C. Y. Lee, T. S. Chin, *Electrochim. Acta* **2007**, *52*, 5407.

[17] L. Ye, M. Liao, H. Sun, Y. Yang, C. Tang, Y. Zhao, L. Wang, Y. Xu, L. Zhang, B. Wang, F. Xu, X. Sun, Y. Zhang, H. Dai, P. G. Bruce, H. Peng, *Angew. Chem. Int. Ed.* **2019**, *58*, 2437.

[18] Q. Chen, J. Jin, Z. Kou, C. Liao, Z. Liu, L. Zhou, J. Wang, L. Mai, *Small* **2020**, 16, 2000091.

[19] L. Wang, K.-W. Huang, J. Chen, J. Zheng, *Sci. Adv.* **2019**, 5, eaax4279.

[20] a) Z. Wang, J. Huang, Z. Guo, X. Dong, Y. Liu, Y. Wang, Y. Xia, *Joule* **2019**, *3*, 1289; b) W. Li, K. Wang, M. Zhou, H. Zhan, S. Cheng, K. Jiang, *ACS Appl. Mater. Interfaces* **2018**, *10*, 22059; c) W. Li, K. Wang, S. Cheng, K. Jiang, *Adv. Energy Mater.* **2019**, *9*, 1900993; d) T. Xiong, Y. Zhang, Y. Wang, W. S. V. Lee, J. Xue, *J. Mater. Chem. A* **2020**, *8*, 9006; e) D. Chao, C. Zhu, M. Song, P. Liang, X. Zhang, N. H. Tiep, H. Zhao, J. Wang, R. Wang, H. Zhang, H. J. Fan, *Adv. Mater.* **2018**, *30*, 1803181; f) S. Cai, X. Chu, C. Liu, H. Lai, H. Chen, Y. Jiang, F. Guo, Z. Xu, C. Wang, C. Gao, *Adv. Mater.* **2021**, *33*, 2007470; g) N. Zhang, F. Cheng, Y. Liu, Q. Zhao, K. Lei, C. Chen, X. Liu, J. Chen, *J. Am. Chem. Soc.* **2016**, *138*, 12894.

[21] L. Martínez, R. Andrade, E. G. Birgin, J. M. Martínez, *J. Comput. Chem.* **2009**, *30*, 2157.

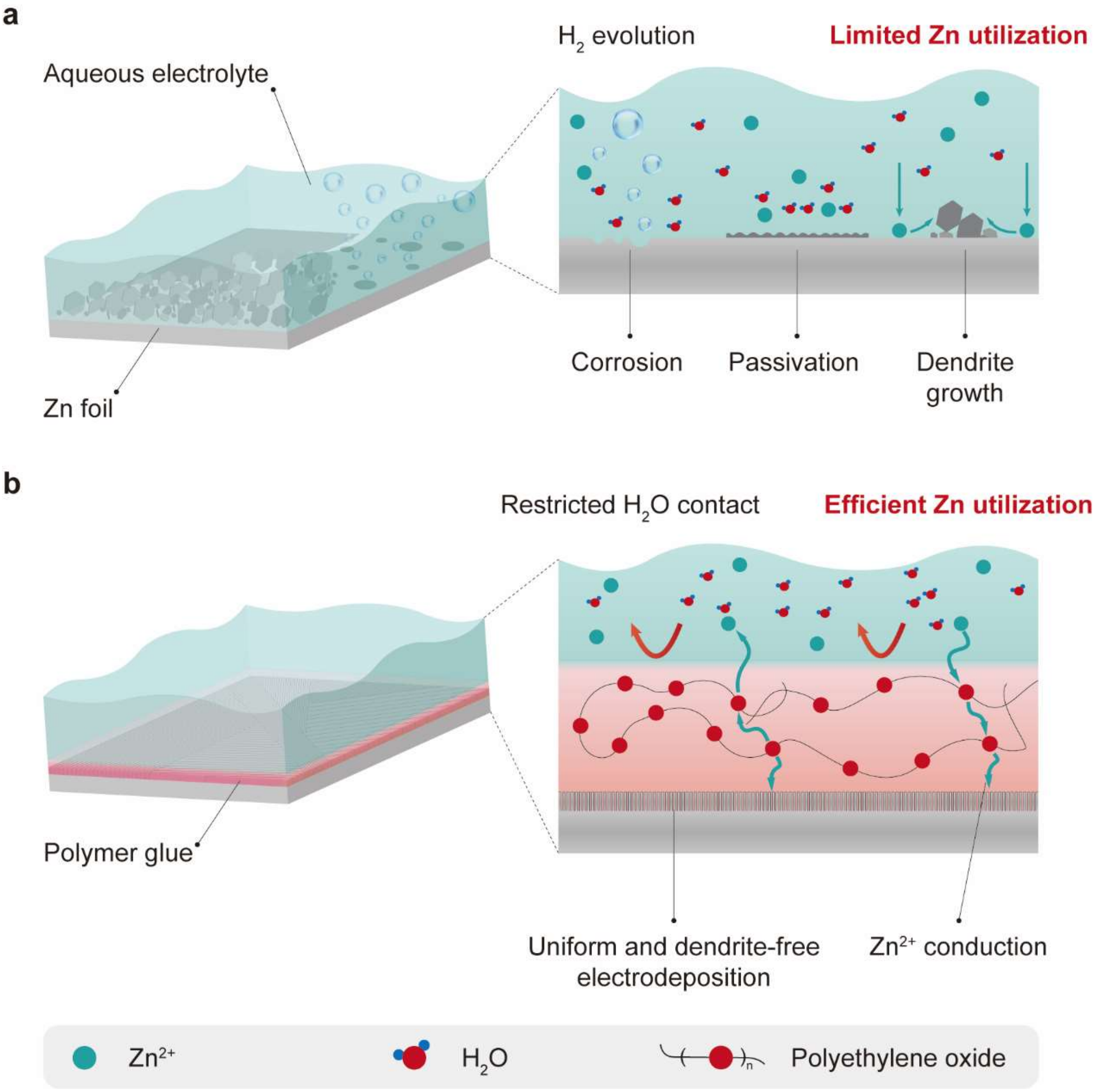

**Figure 1. Schematic diagrams of the reversible Zn utilization. a)** $H_2$ evolution upon corrosion of Zn, passive layer formation, and dendrite growth occur during the deposition in aqueous electrolyte, resulting in restrained Zn utilization. **b)** Polymer glue effectively separates the aqueous electrolyte and Zn foil to inhibit corrosion and passivation while enabling rapid $Zn^{2+}$ ion migration. Besides, polymer glue enables unique uniform dendrite-free electrodeposition to suppress dendrite growth, allowing ultrahigh Zn utilization rate.

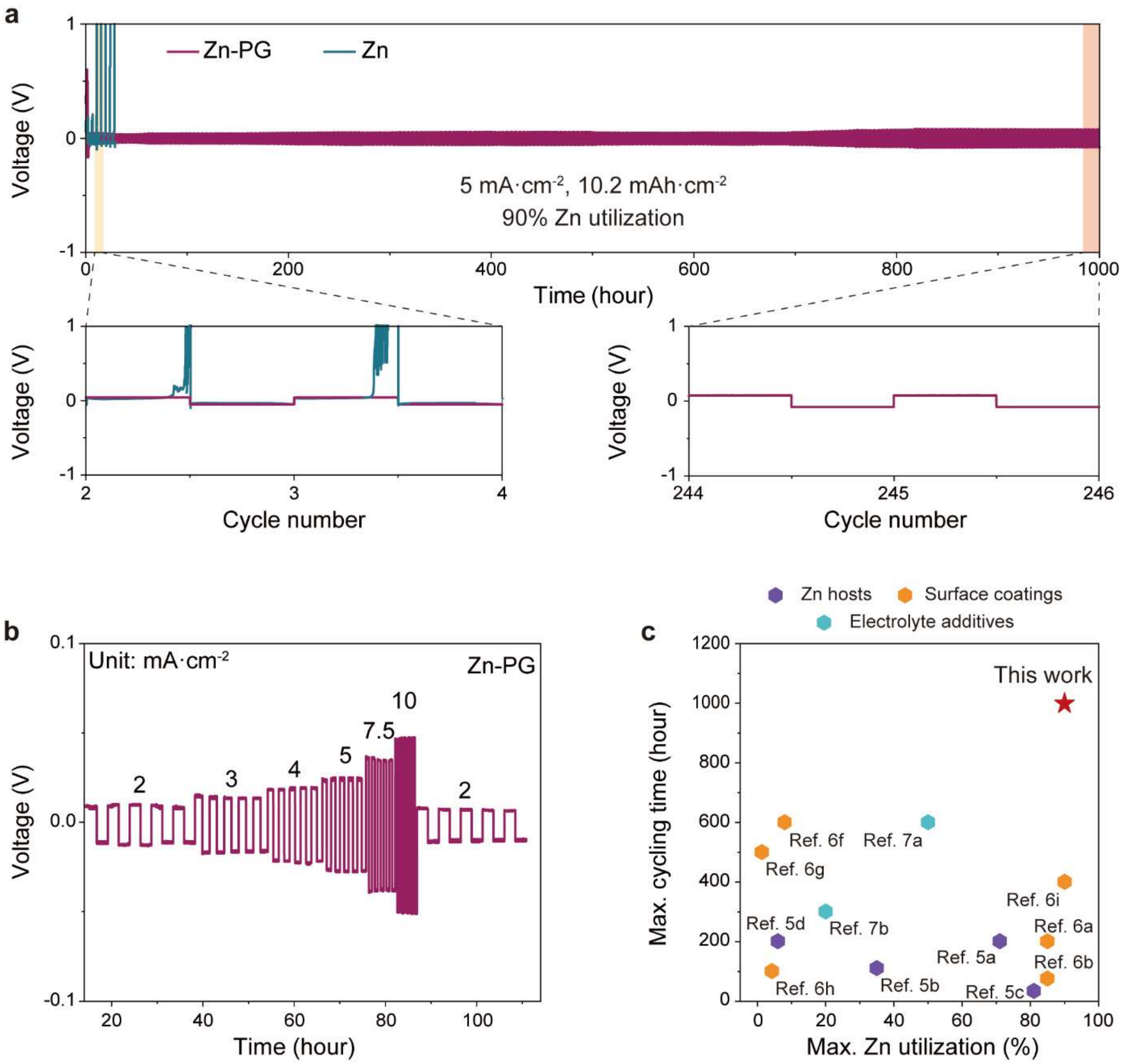

**Figure 2. Electrochemical performance of Zn anodes in symmetric batteries protected by the polymer glue (denoted as PG in Figures, the same below). a)** Galvanostatic charge-discharge curves of symmetric batteries based on polymer glue-coated and bare Zn foils at the current density of 5 mA·cm$^{-2}$ under 90% Zn utilization rate. **b)** Rate performance of symmetric batteries from polymer glue-coated Zn foil at increasing current densities of 2, 3, 4, 5 and 7.5 to 10 mA·cm$^{-2}$ under 80% Zn utilization rate. **c)** Comparison of the performance in Zn utilization rate and cycling time of this work with other reports using porous Zn,[5a] Zn@CNT,[5b] Zn@CNT,[5c] and Zn(002)[5d] Zn hosts; Zn@PI,[6a] Zn@PA,[6b] Zn@ZnF$_2$,[6f] Zn@ZnO,[6g] Zn@ZnO,[6h] and Zn@ILG[6i] surface coatings; acetonitrile[7a] and P444(2O1)-TFSI[7b] electrolyte additives.

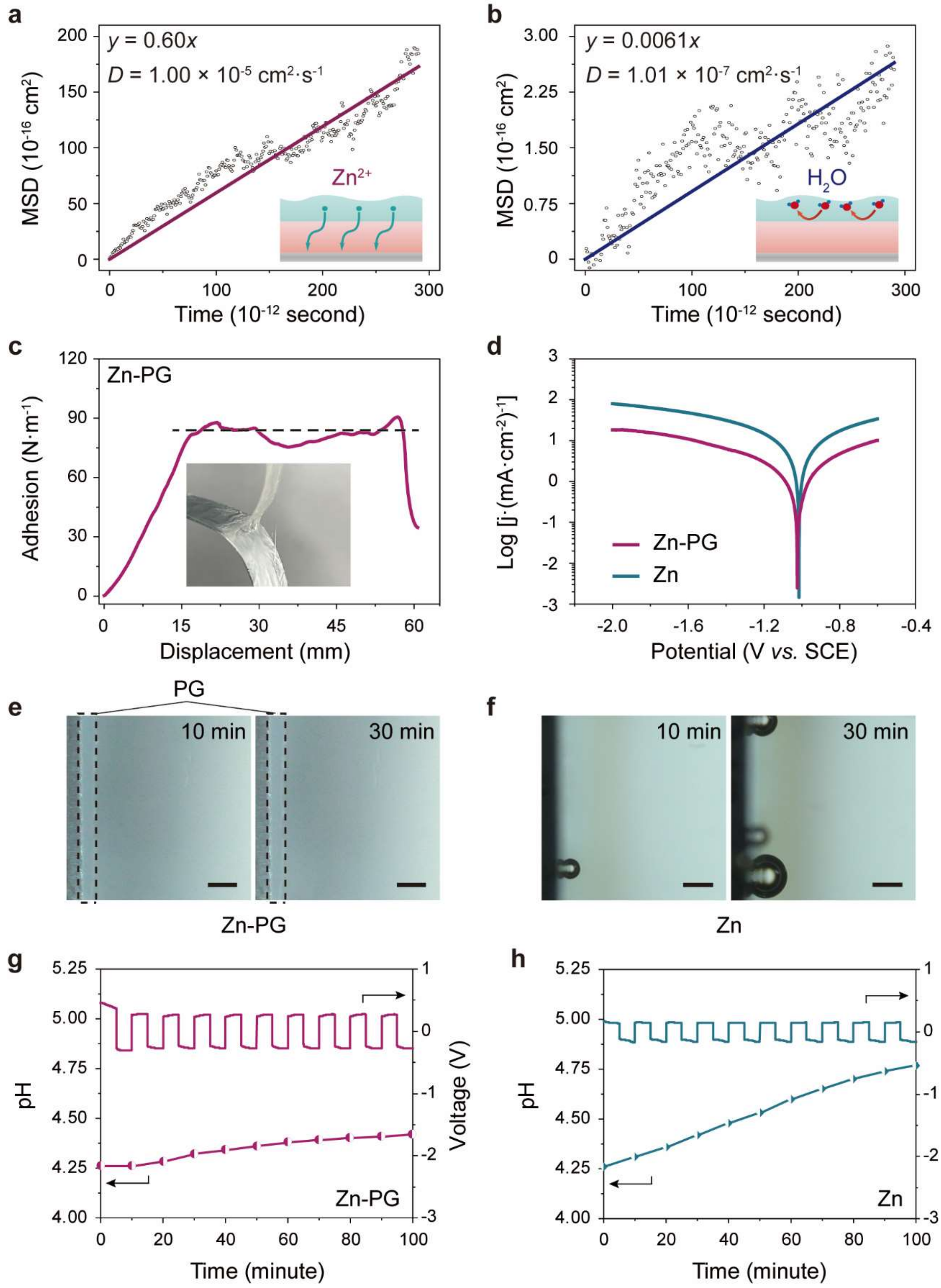

**Figure 3. Characterizations of the anti-corrosion behavior of the polymer glue. a**, **b)** Simulated mean square displacement (denoted as MSD in Figures) of $Zn^{2+}$ and $H_2O$ in polymer glue as a function of simulated time, respectively. **c)** Pull-off adhesion test of Zn foil and polymer glue. **d)** Linear polarization curves of Zn foils in 2 M $ZnSO_4$ electrolyte. **e**, **f)** Cross-sectional optical micrographs of polymer glue-protected Zn foil and bare Zn soaked in 2 M $ZnSO_4$ at a timescale of 30 minutes, respectively. Scale bar: 200 µm. **g**, **h)** pH monitoring of electrolyte of symmetric batteries based on polymer glue-coated and bare Zn anodes at the current density of 5 $mA \cdot cm^{-2}$, respectively.

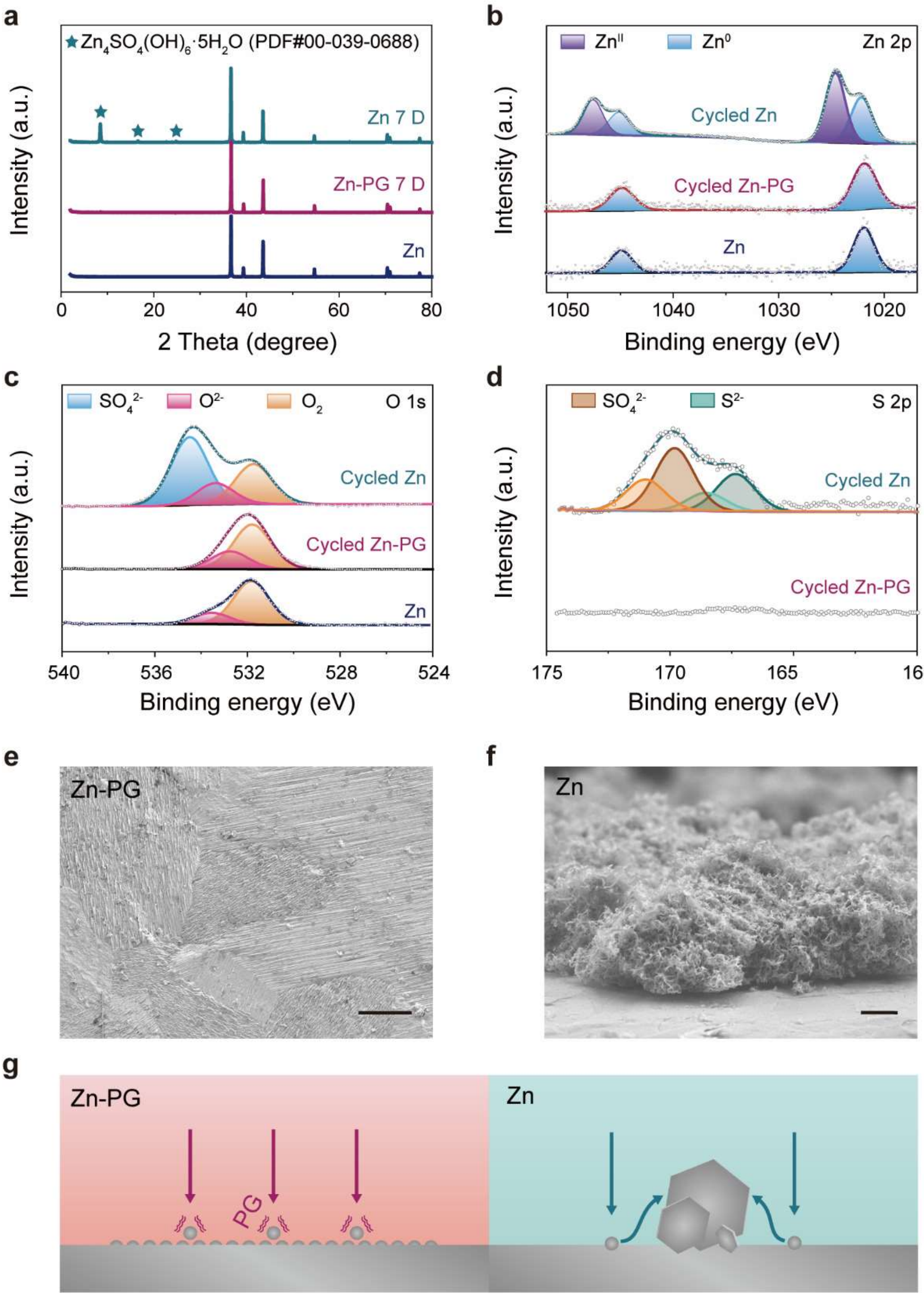

**Figure 4. Characterizations of the anti-passivation and anti-dendrite growth behaviors of the polymer glue.** **a)** X-ray diffraction patterns of pristine and soaked Zn foils in 2 M $ZnSO_4$ for seven days. **b-d)** Zn 2p, O 1s and S 2p X-ray photoelectron spectroscopy curves of pristine Zn foil and cycled Zn anodes, respectively. **e**, **f)** Scanning electron microscopy images of the surface morphology of cycled Zn anodes. Scale bar: 10 µm. **g)** Schematic diagram of the Zn deposition on the Zn anode.

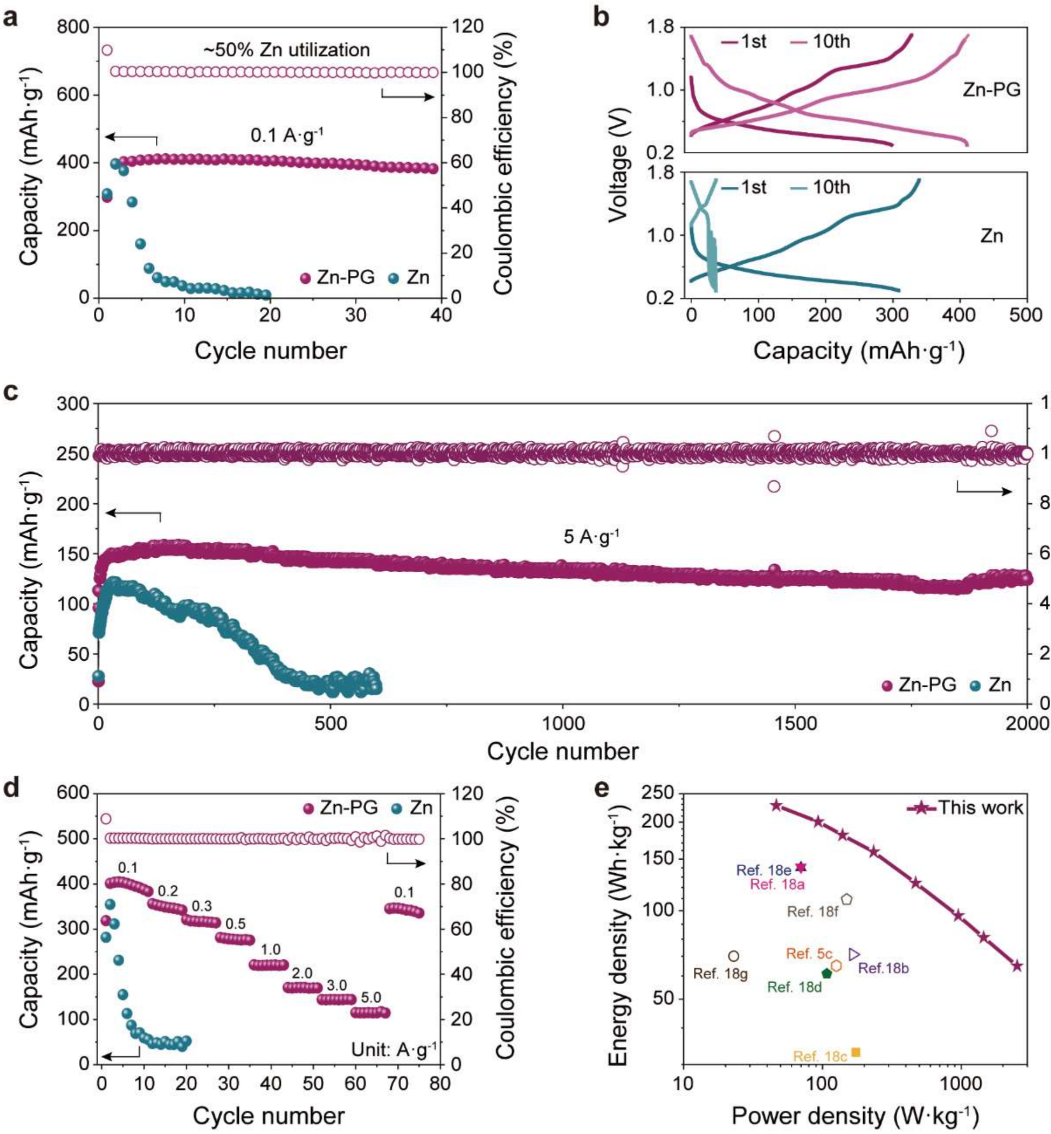

**Figure 5. Electrochemical performance of the full Zn-ion batteries from $NH_4V_4O_{10}$ and Zn. a)** Cycling performance of the Zn-ion batteries based on polymer glue-coated Zn and bare Zn anodes at a current density of 0.1 A·g$^{-1}$. **b)** The 1st and 10th voltage profiles selected from **a**. **c)** Cycling performance of Zn-ion batteries at the current density of 5.0 A·g$^{-1}$. **d)** Rate performance of Zn-ion batteries at increasing current densities of 0.1, 0.2, 0.3, 0.5, 1.0, 2.0 and 3.0 to 5.0 A·g$^{-1}$. **e)** Ragone plots showing the comparison of energy and power densities of this work with the other reports using $MnO_2$-Zn@CNT foam,[5c] AC-Zn@ZIF-800,[20a] NVPF@C-Zn@C,[20b] $ZnMn_2O_4$-$Na_{0.14}TiS_2$,[20c] $Zn_{0.2}MnO_2$-h-$MoO_3$,[20d] $Zn_2(OH)VO_4$-Zn,[20e] Graphene-Zn,[20f] and $ZnMn_2O_4$@C-Zn.[20g]

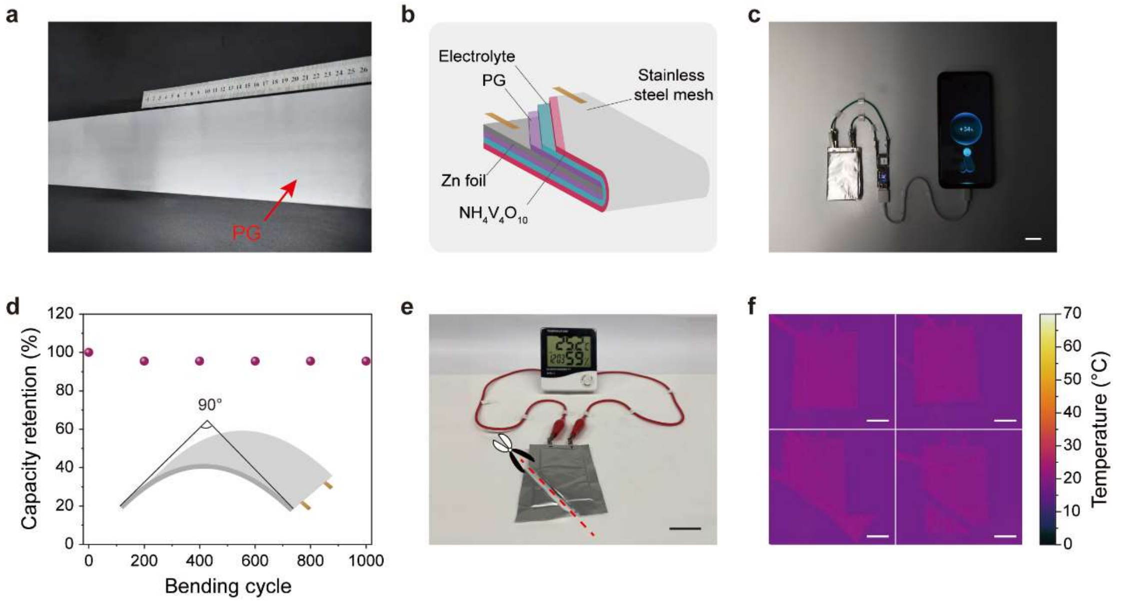

**Figure 6. An outlook for practical applications. a)** Photograph of a large polymer glue-coated Zn foil. **b)** Schematic diagram of the as-fabricated pouch cell. **c)** Photograph of a pouch cell made of $NH_4V_4O_{10}$ and polymer glue-coated Zn foil powering a smartphone. Scale bar: 2 cm. **d)** Capacity retention at difference bending cycles at 90°. The inset diagram depicts the bending deformation applied. **e)** Photograph of a pouch cell made of $NH_4V_4O_{10}$ and polymer glue-coated Zn foil powering a liquid-crystal display after cutting. Scale bar: 2 cm. **f)** Thermal imaging photographs showing the temperature variation of the pouch cell during and after cutting. Scale bar: 2 cm.

## The Table of Contents

A new polymer glue is designed to simultaneously solve the problems of corrosion, passivation and dendrite growth for zinc anode. The modified Zn anode demonstrates 90% Zn utilization at 5 mA·cm$^{-2}$ for 1,000 hours. Full zinc-ion batteries are further made to show ultrahigh energy density of 228 Wh·kg$^{-1}$ based on the total mass of cathode and anode, superior rate performance and long lifespan.

*Yiding Jiao, Fangyan Li, Xin Jin, Qingsong Lei, Luhe Li, Lie Wang, Tingting Ye, Er He, Jiacheng Wang, Hao Chen, Jiang Lu, Rui Gao, Qianming Li, Chang Jiang, Jianwei Li, Guanjie He, Meng Liao, Huigang Zhang, Ivan P. Parkin, Ye Zhang,* and Huisheng Peng**

### Engineering polymer glue towards 90% zinc utilization for 1,000 hours to make high-performance Zn-ion batteries